Molecular Crystals and Liquid Crystals Science and Technology. Section A. Molecular Crystals and Liquid Crystals

Publication details, including instructions for authors and subscription information:
http://www.tandfonline.com/loi/gmcl19

Twisting Transition in a Capillary Filled with Chiral Smectic C Liquid Crystal

D. W. Cronin [a], E. M. Terentjev [a b], R. A. Sones [a] & R. G. Petschek [a]

[a] Department of Physics, Case Western Reserve University, Cleveland, OH, 44106-7079, USA

[b] Cavendish Laboratory, University of Cambridge, Cambridge, CB3 OHE, England

Version of record first published: 04 Oct 2006.

To cite this article: D. W. Cronin , E. M. Terentjev , R. A. Sones & R. G. Petschek (1994): Twisting Transition in a Capillary Filled with Chiral Smectic C Liquid Crystal, Molecular Crystals and Liquid Crystals Science and Technology. Section A. Molecular Crystals and Liquid Crystals, 238:1, 167-177

To link to this article: http://dx.doi.org/10.1080/10587259408046925

Mol. Cryst. Liq. Cryst., 1994, Vol. 238, pp. 167–177
Reprints available directly from the publisher
Photocopying permitted by license only

Printed in the United States of America

Twisting Transition in a Capillary Filled with Chiral Smectic C Liquid Crystal

D. W. CRONIN, E. M. TERENTJEV,† R. A. SONES and R. G. PETSCHEK
Department of Physics, Case Western Reserve University, Cleveland, OH 44106-7079, USA

(Received September 7, 1992; in final form February 15, 1993)

We consider a cylindrical capillary filled with the chiral smectic C phase of a liquid crystal. The smectic layers are stacked along the capillary axis, and at the capillary wall the director is assumed to be parallel to the wall. Non-chiral materials in these conditions exhibit a disclination line which coincides with the capillary axis. In chiral smectic C material the tendency for macroscopic twist competes with the boundary conditions at the wall, and the disclination line can shift away from the capillary axis and form a helix. We calculate an approximate phase diagram for the system, which shows how the phase (helical or non-helical) depends on material parameters (elastic constants and chirality) and capillary radius. Both continuous and discontinuous phase transitions occur: the continuous transition should be observable in ordinary liquid crystals, while the discontinuous transition should be observable in main chain polymer liquid crystals. Observation of the discontinuous transition would provide information about a poorly known elastic constant.

Keywords: smectic C, disclination, confined geometry*

I. INTRODUCTION

Liquid crystal molecules typically have rod-like shapes and can exhibit various liquid crystalline phases. In the nematic phase[1,2,3] the rod-like molecules tend to orient along a particular direction (described by the unit vector $\hat{\mathbf{n}}$, called the director), but there remains full translational symmetry. At lower temperatures smectic A and C phases may appear, where the molecules are stacked in flat layers and show a high degree of orientational ordering, but have no positional ordering within a given layer.[3] In the smectic A phase the director is normal to the layers, while in the smectic C phase it tilts slightly from the layer normal. The smectic C geometry is depicted in Figure 1, where θ denotes the tilt angle (typically zero to ten degrees), $\mathbf{c}$ is the component of $\hat{\mathbf{n}}$ parallel to the layers, and the polarization vector $\mathbf{p} \equiv \hat{\mathbf{z}} \times \mathbf{c}$ is also parallel to the layers and perpendicular to both $\hat{\mathbf{n}}$ and $\mathbf{c}$. If the molecules are non-centrosymmetric, then a chiral smectic C phase (denoted C*) may occur, where the director not only tilts but also tends to rotate about the layer normal as

†Present address: Cavendish Laboratory, University of Cambridge, Cambridge CB3 0HE, England.

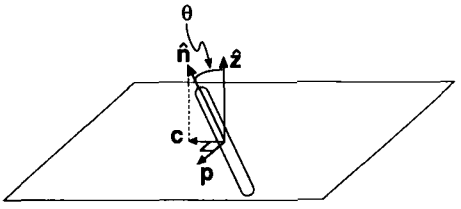

FIGURE 1 Relationship between the layer normal $\hat{\mathbf{z}}$, director $\hat{\mathbf{n}}$, polarization vector $\mathbf{p}$, and $\mathbf{c}$.

one moves from layer to layer, with a typical wave number (in bulk material) of $q^* \sim 10^4\ \text{cm}^{-1}$.

A main chain polymer liquid crystal molecule is composed of a chain of rod-like mesogens connected head-to-tail by semiflexible spacers. The mesogens can exhibit the same liquid crystalline phases described above; in the smectic phases, the semiflexible spacers reside between neighboring layers.

We will consider a smectic C* liquid crystal (or main chain liquid crystal polymer) confined within a cylindrical capillary, with the smectic layers stacked along the capillary axis, and the director parallel to the capillary wall, at the wall. If the material is not chiral there is a singular line of 2π-disclination in the director field coincident with the capillary axis. In a chiral material the tendency for macroscopic twist competes with the boundary conditions at the wall. We will consider the possibility that the disclination shifts away from the capillary axis and forms a helix, and will assume a form of the director field which is consistent with the helical disclination and the boundary conditions at the wall. Then we will minimize the system free energy with respect to the radius and wave number of the helix, and calculate an approximate phase diagram for the system which shows how the phase (helical or non-helical) depends on material parameters (elastic constants and chirality) and capillary radius, and reveals the existence of both continuous and discontinuous phase transitions.

II. THEORY

Consider a smectic C* liquid crystal polymer confined within a cylindrical capillary, with the smectic layers stacked along the capillary axis (z-axis). Assume that the smectic layers are ideal and that the tilt angle θ is spatially uniform. Then the free energy density may be written[4,5]

$$\mathcal{F} = \frac{K_1 c^2}{2}(\nabla\cdot\hat{\mathbf{c}}) + \frac{K_2 c^2}{2}(\hat{\mathbf{c}}\cdot\nabla\times\hat{\mathbf{c}} + q^*)^2 + \frac{K_3 c^2}{2}(\hat{\mathbf{z}}\cdot\nabla\times\hat{\mathbf{c}})^2$$

$$- K_4 c^3(\hat{\mathbf{c}}\cdot\nabla\times\hat{\mathbf{c}} + q^*)(\hat{\mathbf{z}}\cdot\nabla\times\hat{\mathbf{c}}), \quad (1)$$

where $c \equiv |\mathbf{c}| = \sin(\theta) << 1$, and the K's are elastic constants. The stability of the

smectic C structure imposes the constraints $K_1, K_2, K_3 > 0$ and $K_2K_3 > c^2K_4^2$.[4] If $\bar{\phi}$ is the angle between $\mathbf{c}$ and $\hat{\mathbf{x}}$, then

$$\hat{\mathbf{c}} = \cos(\bar{\phi})\hat{\mathbf{x}} + \sin(\bar{\phi})\hat{\mathbf{y}}, \tag{2}$$

where $\hat{\mathbf{c}}$ is a unit vector along $\mathbf{c}$. The orientation angle $\bar{\phi}$ is a scalar field and $\hat{\mathbf{c}}$ is a vector field.

The polarization vector makes an angle $\phi = \bar{\phi} + \pi/2$ with $\hat{\mathbf{x}}$. The fields $\mathbf{c}$ and $\mathbf{p}$ contain the same information, but $\mathbf{p}$ will be more convenient for our purposes. Substituting Equation (2) into Equation (1) and expressing the result in terms of ϕ gives

$$\mathcal{F} = \frac{K_1c^2}{2}[\cos(\phi)\phi_x + \sin(\phi)\phi_y]^2 + \frac{K_2c^2}{2}(\phi_z - q^*)^2$$

$$+ \frac{K_3c^2}{2}[\sin(\phi)\phi_x - \cos(\phi)\phi_y]^2 - K_4c^3(\phi_z - q^*)[\sin(\phi)\phi_x - \cos(\phi)\phi_y], \tag{3}$$

where $\phi_x \equiv \partial\phi/\partial x$ and so forth. In bulk material the free energy (the volume integral of $\mathcal{F}$) is minimized by the uniform rotation $\phi(x, y, z) = q^*z$. In the capillary, one could in principle solve for the field $\phi(x, y, z)$ which minimizes the integral of $\mathcal{F}$ over the capillary volume, subject to boundary constraints at the capillary wall. We will use a simpler, approximate method of solution: we will guess a physically plausible field $\phi(x, y, z)$ which satisfies the boundary constraints and depends on two adjustable parameters, and then minimize with respect to these parameters.

A. Free Energy of Helical Configuration

We assume that, at the capilary wall, $\mathbf{p}$ is normal to the wall; this is the same boundary condition as in a Clark-Lagerwall cell.[6] Liquid crystal polymers satisfy this boundary condition because of steric effects, while ordinary liquid crystals require appropriate surface preparation.

If the smectic C material in the capillary is non-chiral ($q^* = 0$), the solution which minimizes the free energy is well known (see Figure 2a): the $\mathbf{p}$-field is radial, with $\phi(x, y, z) = \arctan(y/x)$. There is a singularity (2π-disclination) along the capillary axis, corresponding to a filamentary core of 'melted' material.[7,8] This core has free energy per unit length F_c and a circular cross-section of radius $\rho_0 \sim 10^{-6}$ cm.

When chirality is introduced the solution may change. It is plausible that a chiral material may reduce its free energy if the melted core forms a helix around the capillary axis (see Figure 2b). We parameterize the helix by its radius a and wave number q, and note that the non-helical solution corresponds to $a = 0$. We also assume, for concreteness and simplicity, that F_c and ρ_0 are independent of a and q, and that the core's cross-section perpendicular to $\hat{\mathbf{z}}$ remains circular.

Consider the $z = 0$ plane. Let $\phi_0(x, y) \equiv \phi(x, y, 0)$ denote the orientation angle of the vector field $\mathbf{p}(x, y, 0)$, and let the disclination point be located at $(a, 0, 0)$.

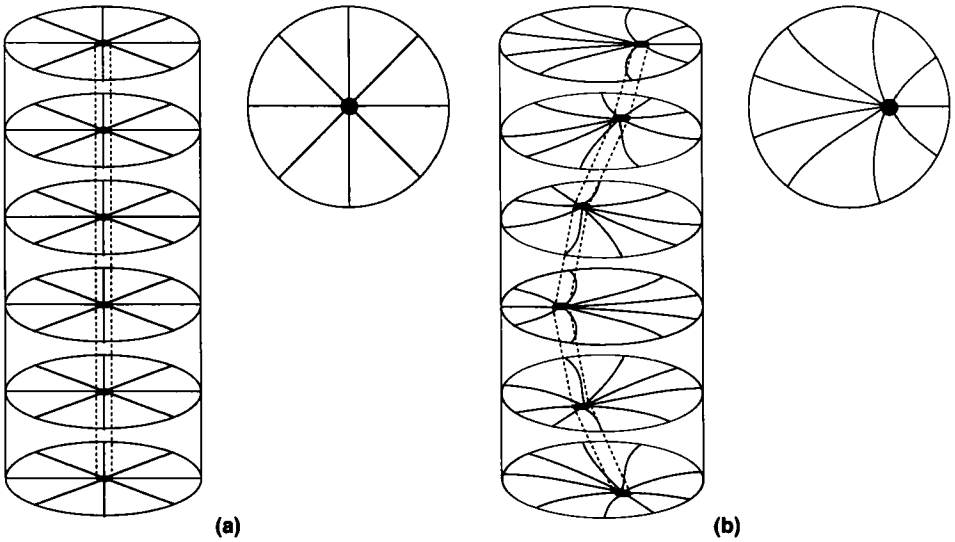

FIGURE 2 Sketch of the (a) non-helical and (b) helical configurations. The outer cylinder represents the capillary wall and the thin inner tube (dashed lines) is the melted core. Lines radiating from the core represent the **p**-field. Also shown are cross-sections of the capillary, corresponding to a single smectic C layer.

Since the disclination is a helix with locus $(a\cos(qz), a\sin(qz), z)$, as we move away from the $z = 0$ plane the $\phi_0(x, y)$ field rotates, giving

$$\phi(x, y, z) = \phi_0(u, v) + qz, \tag{4}$$

where

$$u \equiv x\cos(qz) + y\sin(qz)$$

$$v \equiv -x\sin(qz) + y\cos(qz).$$

Note that

$$\phi_z(x, y, 0) = q[1 - x\phi_{0y}(x, y) + y\phi_{0x}(x, y)]. \tag{5}$$

The free energy per unit length of the capillary is

$$F = F_c\sqrt{1 + q^2a^2} + \iint_{\mathcal{A}'} \mathcal{F}(x, y, 0)\, dx\, dy, \tag{6}$$

where $\mathcal{A}$ denotes the cross-sectional area of the capillary excluding the melted core region at $(a, 0, 0)$, and we evaluate $\mathcal{F}(x, y, z)$ at $z = 0$ for convenience, since a uniform helix must have F independent of z. The square root factor is the path

length along the helix per unit path length along the capillary axis. The free energy per unit length of the non-helical configuration is

$$F_0 = F_c + \iint_{\mathcal{A}'} \mathcal{F}_0(x, y)\, dx\, dy, \tag{7}$$

where $\mathcal{F}_0(x, y)$ is the free energy density of the non-helical configuration and $\mathcal{A}'$ denotes the cross-sectional area of the capillary minus that of the melted core at $(0, 0, 0)$.

B. Electrostatic Analogy for p-Field

The fact that $\mathbf{p}(x, y, 0)$ is singular at $(a, 0, 0)$ and normal to the capillary wall suggests an electrostatic analogy. Think of the capillary as a hollow conducting cylinder with a line of uniform charge density passing through $(a, 0, 0)$ and parallel to $\hat{\mathbf{z}}$. This well-known electrostatic problem can be solved by the method of images, giving for the orientation angle of the electric field

$$\tan(\phi_0) = \frac{y[(a - x) + (1/a - x)]}{y^2 - (a - x)(1/a - x)}, \tag{8}$$

where all distances are expressed in units of the capillary radius. We will use this expression for the orientation angle of $\mathbf{p}$ in the $z = 0$ plane. Equations (4) and (8) completely determine $\phi(x, y, z)$ in terms of the parameters a and q.

Substitute $\phi(x, y, z)$ from Equations (4) and (8) into Equation (3) to get

$$\mathcal{F}(x, y, 0) = \frac{K_1 c^2}{2} I_1^2 + \frac{K_2 c^2}{2} (qI_2 - q^*)^2 + \frac{K_3 c^2}{2} I_3^2 - K_4 c^3 (qI_2 - q^*) I_3, \tag{9}$$

where

$$I_1^2 \equiv [\cos(\phi_0)\phi_{0x} + \sin(\phi_0)\phi_{0y}]^2 = \frac{4y^2}{[(a - x)^2 + y^2][(1/a - x)^2 + y^2]}$$

$$I_2 \equiv \frac{\phi_z(x, y, 0)}{q} = \frac{(1 - x^2 - y^2)[1 - (a + 1/a)x + x^2 + y^2]}{[(a - x)^2 + y^2][(1/a - x)^2 + y^2]}$$

$$I_3 \equiv \sin(\phi_0)\phi_{0x} - \cos(\phi_0)\phi_{0y} = -\frac{(a - x) + (1/a - x)}{\sqrt{[(a - x)^2 + y^2][(1/a - x)^2 + y^2]}}.$$

The free energy density of the non-helical configuration (let $a \to 0$ in Equation (9)) is

$$\mathcal{F}_0(x, y) = \frac{K_2 c^2}{2} (q^*)^2 + \frac{K_3 c^2}{2} I_0^2 + K_4 c^3 q^* I_0, \tag{10}$$

where

$$I_0 \equiv \lim_{a \to 0} I_3 = -\frac{1}{\sqrt{x^2 + y^2}}.$$

The difference in free energy per unit length between the helical and non-helical configurations is (see Appendix)

$$\frac{\Delta F}{\pi c^2} = \left(K_1 - \frac{8K_4 cq}{3}\right) \ln\left(\frac{1}{1 - a^2}\right) + \frac{K_2 \ln(1/\rho_0)}{2} q^2 a^2 - K_2 q^* q a^2. \quad (11)$$

The F_c term is negligible compared to the q^2a^2 term and has been discarded, since typical materials have $F_c/(\pi c^2) \ll K_2 \ln(1/\rho_0)$ when the melted core is smectic A, which we assume.[5]

Equation (11) is our central result. If ΔF is negative for some q and a, then the corresponding helix is favored over the non-helical configuration. Note that ΔF is invariant under the transformation $a \to -a$, as expected for a helix.

III. RESULTS AND DISCUSSION

Minimizing ΔF with respect to q in Equation (11) gives

$$q = \tilde{q}\left(1 + \frac{\gamma}{a^2} \ln\left(\frac{1}{1 - a^2}\right)\right), \quad (12)$$

where

$$\tilde{q} \equiv \frac{q^*}{\ln(1/\rho_0)}$$

$$\gamma \equiv \frac{8K_4 c}{3K_2 q^*}.$$

Substituting this expression for q into Equation (11) gives

$$\Delta f(a) \equiv \frac{\alpha}{K_1} \frac{\Delta F}{\pi c^2} = \alpha \ln\left(\frac{1}{1 - a^2}\right) - a^2 \left(1 + \frac{\gamma}{a^2} \ln\left(\frac{1}{1 - a^2}\right)\right)^2, \quad (13)$$

where

$$\alpha \equiv \frac{2K_1 \ln(1/\rho_0)}{K_2 (q^*)^2}.$$

Since K_1, K_2 and c are positive, so is α, and the signs of $\tilde{q}$ and γ depend on the signs of q^* and K_4. The parameters $\tilde{q}$, γ and α are dimensionless, while ρ_0 and q^* are expressed in terms of the capillary radius. To express ρ_0 and q^* in dimensional form, let $\rho_0 \rightarrow \rho_0/R$ and $q^* \rightarrow q^*R$, where R is the capillary radius.

Within the context of our model the maximum permissible value of a is $a_m = 1 - \rho_0$, corresponding to the disclination touching the capillary wall. Thus we must minimize $\Delta f(a)$ over the range $0 \leq a \leq a_m$.

First consider the case when γ is zero. (This case is relevant, for example, near the smectic C to smectic A transition, where $c \rightarrow 0$.) Then the minimization of $\Delta f(a)$ is readily performed: $a = \sqrt{1 - \alpha}$ for $\alpha < 1$, and $a = 0$ otherwise; and $q = \tilde{q}$ for all α. There is a continuous (second order) transition from the non-helical to the helical configuration as α drops below 1. For a typical material with $K_1 \sim K_2$, $\rho_0 \sim 10^{-6}$ cm and $q^* \sim 10^4$ cm^{-1}, the transition occurs for a capillary radius $R \sim 10^{-4}$ cm, which is experimentally accessible. The corresponding wave number is $\tilde{q} \sim 10^4$ cm^{-1}. Greater chirality (larger q^*) and bigger capillary radius favor the appearance of the helix.

If γ is non-zero, $\Delta f(a)$ exhibits rich behavior, including discontinuous (first order) transitions. Figure 3 shows $\Delta f(a)$ versus a for particular values of ρ_0/R and α, and several values of γ. Note, for example, that as γ changes from -0.5 to -0.75 there is a discontinuous transition from a non-helical configuration to a maximum-radius helix.

Figure 4 is a phase diagram of the order parameter a, showing the boundaries of the stable and metastable configurations in (α, γ) parameter space. Despite its

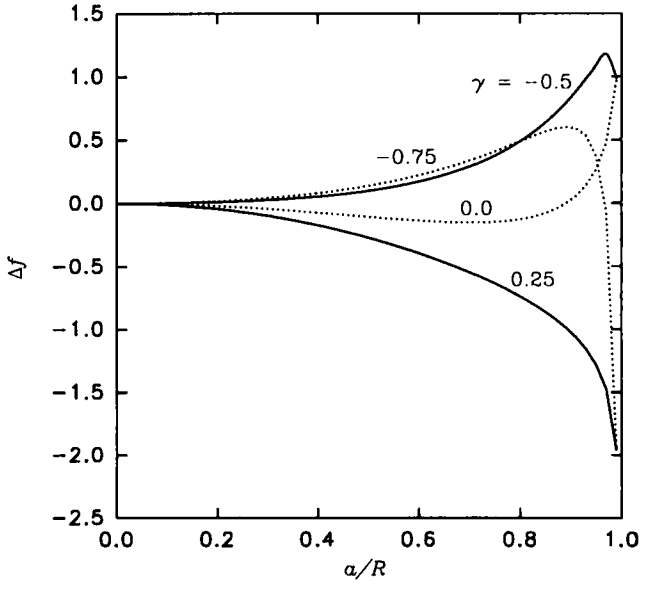

FIGURE 3 Plots of $\Delta f(a)$ versus a for $\rho_0/R = 0.01$, $\alpha = 0.5$ and several values of γ. For $\gamma = 0.25$ the stable configuration is a maximum-radius helix ($a/R = 0.99$) with the disclination touching the wall; for $\gamma = 0$ the stable configuration is a helix with $a/R \simeq 0.71$; for $\gamma = -0.5$ the stable configuration is non-helical ($a/R = 0$), and there is also a metastable maximum-radius helix; and for $\gamma = -0.75$ the stable configuration is a maximum-radius helix, and there is also a metastable non-helical configuration.

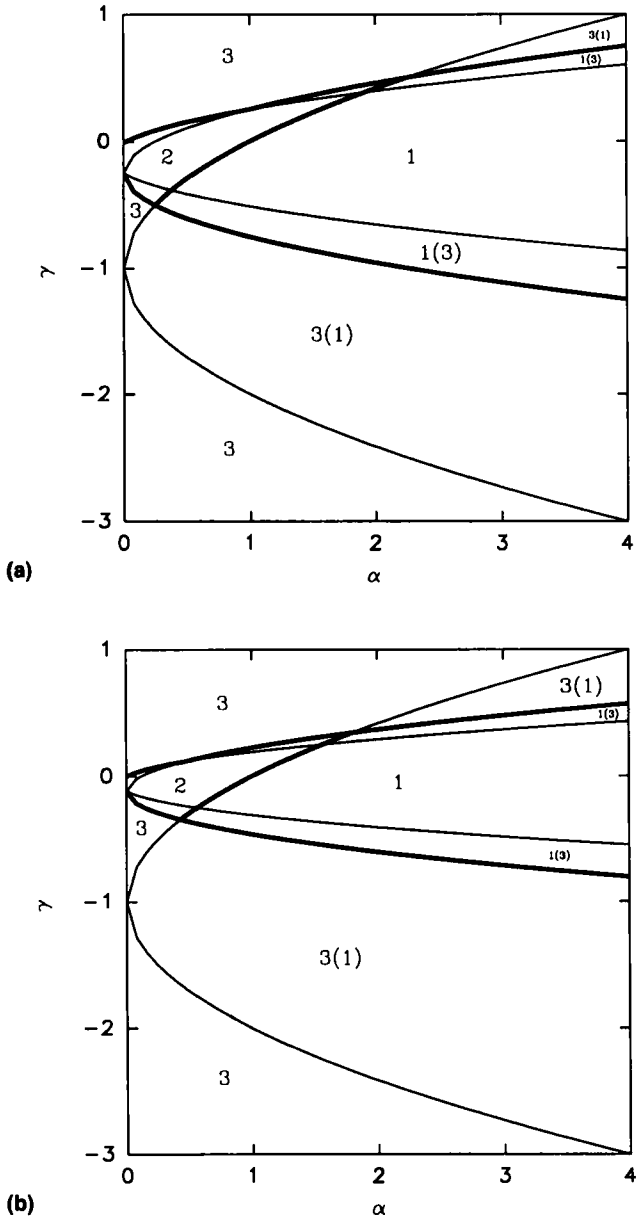

FIGURE 4 Phase diagram of the order parameter a for (a) $\rho_0/R = 0.01$ and (b) $\rho_0/R = 0.0001$. The thick lines are boundaries between stable configurations, and the thin lines border regions where metastable configurations can exist. Region 1 corresponds to a non-helical configuration ($a = 9$); region 2 a helix ($0 < a < a_m$); and region 3 a maximum-radius helix ($a = a_m$). A region such as 3(1) corresponds to a stable maximum-radius helix or a metastable non-helical configuration. The small unlabeled regions surrounding region 2 are of type 2(3).

apparent complexity, this phase diagram can be calculated fairly easily for $\Delta f(a)$ and its derivatives. Since $\Delta f'(0) = 0$, existence of a non-helical configuration (stable or metastable) is determined by $\Delta f''(0) > 0$, which gives

$$-1 - \sqrt{\alpha} < \gamma < -1 + \sqrt{\alpha}.$$

Existence of a maximum-radius helix (stable or metastable) is determined by $\Delta f'(a_m) < 0$, which gives

$$\gamma > -\mu + \mu\sqrt{1 - (1 - a_m^2 - \alpha)/\mu} \text{ or } \gamma < -\mu - \mu\sqrt{1 - (1 - a_m^2 - \alpha)/\mu},$$

where μ is positive and defined by

$$\mu \equiv \frac{-a_m^4}{2a_m^2 \ln(1 - a_m^2) + (1 - a_m^2)\ln^2(1 - a_m^2)}.$$

The non-helical configuration is favored over the maximum-radius helix when $\Delta f(a_m) > 0$, which gives

$$-\nu - \sqrt{\nu\alpha} < \gamma < -\nu + \sqrt{\nu\alpha},$$

where ν is positive and defined by

$$\nu \equiv \frac{-a_m^2}{\ln(1 - a_m^2)}.$$

This condition also favors the non-maximum-radius helix over the maximum-radius helix—a conclusion reached by numerical exploration of Equation (13).

In Figure 4 the thick line between regions 1 and 2 represents a continuous phase transition from a non-helical configuration to a helix; the other two thick lines represent discontinuous transitions to a maximum-radius helix. The regions of metastability may cause hysteresis in the transitions, particularly in polymer systems for which the approach to thermal equilibrium may be slow. For $\rho_0/R = 0.01$ the triple points are (2.25, 0.50) and (0.25, −0.50), and for $\rho_0/R = 0.0001$ they are (1.80, 0.34) and (0.43, −0.34).

The analysis we have given is valid for both polymer and non-polymer smectic C* liquid crystals. In a non-polymer system one expects $|K_4|$ to be less than or of the same order as K_2, while in a main chain polymer system $|K_4|$ can be much larger than K_2.[9] Thus, a main chain polymer system can have much larger $|\gamma|$ than a non-polymer system, which would allow more of the phase space of Figure 4 to be explored. For a typical material with $K_1 \simeq K_2$, $\rho_0 \simeq 10^{-6}$ cm and $q^* \simeq 10^4$ cm^{-1}, the upper triple point in Figure 4a corresponds to $R \simeq 2 \times 10^{-4}$ cm and $K_4c/K_4 \simeq 0.8$, with $q \simeq 5 \times 10^{-3}$ cm^{-1}. This should be experimentally accessible in a main chain polymer liquid crystal. Since c is small (typically 0.2 or less) and the K_4 free energy term is a factor of c smaller than the other elastic terms, it is often neglected in theoretical treatments of liquid crystals. It is interesting that the

discontinuous transitions we predict are entirely dependent on K_4 (recall that γ is proportional to K_4). Experimental confirmation of the phase diagram of Figure 4 would amount to a measurement of K_4.

Acknowledgment

This work was supported through the ALCOM Science and Technology Center by the State of Ohio Department of Development and Board of Regents and the NSF under grant DMR-8920147.

APPENDIX: FREE ENERGY INTEGRALS

From Equations (6), (7), (9) and (10) the difference in free energy per unit length between the helical and non-helical configurations is

$$\Delta F \equiv F - F_0 = F_c(\sqrt{1 + q^2a^2} - 1) + \frac{K_1c^2}{2} J_{11} + \frac{K_2c^2}{2} q^2J_{22}$$

$$- K_2c^2q^*qJ_2 + \frac{K_3c^2}{2} (J_{33} - J_{00}) - K_4c^3qJ_{23} + K_4c^3q^*(J_3 - J_0), \quad \text{(A1)}$$

where, in the limit $\rho_0 \to 0$,

$$J_0 \equiv \iint_{\mathcal{A}'} I_0 \, dx \, dy = -2\pi$$

$$J_{00} \equiv \iint_{\mathcal{A}'} I_0^2 \, dx \, dy = 2\pi \ln(1/\rho_0)$$

$$J_{11} \equiv \iint_{\mathcal{A}} I_1^2 \, dx \, dy = 2\pi \ln[1/(1 - a^2)]$$

$$J_2 \equiv \iint_{\mathcal{A}} I_2 \, dx \, dy = \pi a^2$$

$$J_{22} \equiv \iint_{\mathcal{A}} I_2^2 \, dx \, dy = \pi a^2 \ln(1/\rho_0)$$

$$J_{23} \equiv \iint_{\mathcal{A}} I_2 I_3 \, dx \, dy \simeq (8\pi/3)\ln[1/(1 - a^2)]$$

$$J_3 \equiv \iint_{\mathcal{A}} I_3 \, dx \, dy = -2\pi$$

$$J_{33} \equiv \iint_{\mathcal{A}} I_3^2 \, dx \, dy = 2\pi \ln(1/\rho_0).$$

The integral J_{23} was evaluated numerically, and the given expression reproduces the numerical results to within 3 percent for $0 < a < 0.5$, and 25 percent for $0 < a < 0.99$.

References

1. A. R. Khokhlov and A. N. Semenov, *Usp. Fiz. Nauk* [*Sov. Phys. Uspekhi*, **31**, 988 (1988)].
2. M. Warner, J. M. F. Gunn and A. Baumgartner, *J. Phys.*, **A18**, 3007 (1985).
3. P. G. de Gennes, *Physics of Liquid Crystals*, Clarendon, Oxford (1974).
4. M. J. Stephen and J. P. Straley, *Rev. Mod. Phys.*, **46**, 687 (1974).
5. S. A. Pikin, *Structural Transformations in Liquid Crystals*, Gordon & Breach, New York (1991).
6. N. A. Clark and S. T. Lagerwall, *Appl. Phys. Lett.*, **36**, 899 (1980).
7. J. Fousek and M. Glogarove, *Ferroelectrics*, **53**, 71 (1984).
8. E. B. Loginov and E. M. Terentjev, *Kristallographia* [*Sov. Phys. Crystallography*, **30**, 4 (1985)].
9. R. G. Petschek and E. M. Terentjev, *Phys. Rev.*, **A45**, 930 (1992).